Progress In Electromagnetics Research B, Vol. 48, 249–269, 2013

DESIGN OF ARBITRARY SHAPED PLANAR RESONATORS WITH FINE DETAILS USING MODIFIED SPACE SPECTRAL DOMAIN APPROACH

Essam A. Hashish[1] and Hossam A. Saker[2, *]

[1]Electronics and Communications Department, Faculty of Engineering, Cairo University, Giza, Egypt

[2]Microstrip Department, Electronics Research Institute, Cairo, Egypt

Abstract—Space spectral domain approach (SSDA) is a full-wave analysis method that combines the advantages of the spectral domain analysis (SDA) with that of the one dimensional method of lines (MOL). This approach is very efficient to solve 3D MIC/MMIC circuits with higher convergence, higher accuracy and minimized computation time. However, arbitrary shaped structures involving non-homogenous metallization distribution in the resonator patch could hardly be solved using this method. In this paper, the analysis of the space spectral domain approach (SSDA) is developed using non-equidistant MOL discretization as well as modified current basis functions to reduce the computation time window and to sense also accurately the fine metallization details of arbitrary shaped resonators. The modified SSDA approach is applied to solve ten arbitrary shaped resonators with a reduction of computation time less than 10%. Design curves are also presented for these shapes and good agreement is achieved between numerical and experimental results.

1. INTRODUCTION

Microwave resonators can take different forms and shapes from metallic cavities to planar structures. In the last few decades, the use of planar resonator structures are increasing popularly due to their compatibility with other common fabrication techniques in the semiconductor industry such as integrated circuits [1, 2].

MOL is an efficient method for calculating the dispersion characteristics of planar waveguide structures such as planar microstrip

Received 18 November 2012, Accepted 28 January 2013, Scheduled 29 January 2013

* Corresponding author: Hossam Abd El Maoula Saker (habdelmaoula@tra.gov.eg).

resonators. So far, the MOL has been applied only to rectangular shaped circuit structures [3–6], which are easy to discretize. However, for the two dimensional scheme of the MOL, it is difficult to satisfy all boundary conditions simultaneously for the arbitrary shaped structures. Also, the MOL requires large number of discretization lines to handle structures with fine details [6]. This requires computer-time-intensive algorithm, and leads to lower accuracy and efficiency.

In 1998, MOL was modified by generalized transmission line equations (GTL) for calculating the scattering parameters of 2-D structures that can be divided into cascaded subsections in the propagation direction [7–11]. It is also used for reducing the dielectric and magnetic losses to improve the Q-factor of 2-D resonator structures [12, 13]. But the applications of the method are still limited to structures of rectangular metallization distribution.

The space spectral domain approach (SSDA) is a numerical technique developed to characterize, arbitrarily shaped, spatial three dimensional (3-D) discontinuities in MIC/MMIC circuits [14–16]. This method combines the advantages of the spectral domain analysis (SDA) with that of one dimensional method of lines (MOL). The new approach is numerically very efficient and can be applied to planar transmission lines on isolating as well semiconducting substrates with and without open boundaries. The advantages of this approach are that the discretization in the plane of the resonator patch is performed along one direction only, (e.g., z direction) and the boundary conditions for each discretized line can be easily satisfied along the other direction, (e.g., x direction) using current basis functions.

In this paper, the analysis of the space spectral domain approach (SSDA) is developed by using non-equidistant discretization in the z direction to reduce the computation time window and using also new basis functions along the x direction to satisfy the boundary conditions. It is found that this modified SSDA approach has resulted in a reduction of the computational time by a factor less than 10% when compared to that of the conventional approach.

Design curves for ten different arbitrary shaped resonators with fine details are presented. The numerical results are compared with the experimental data of [17], and it is found that good agreement between both data is achieved.

2. THEORY

2.1. Basic Equations of (SSDA)

Considering an arbitrarily shaped resonator discretized in z-direction as shown in Fig. 1(a), the electromagnetic fields at each line are

expressed by [3]:

$$\vec{E} = -\nabla \times \psi^h \vec{e}_z - j\omega\mu\psi^e \vec{e}_z + \frac{1}{j\omega\varepsilon}\nabla\left(\nabla \cdot \psi^e\right)\vec{e}_z \tag{1}$$

$$\vec{H} = -\nabla \times \psi^e \vec{e}_z - j\omega\varepsilon\psi^h \vec{e}_z + \frac{1}{j\omega\mu}\nabla\left(\nabla \cdot \psi^h\right)\vec{e}_z \tag{2}$$

where:

$$\frac{1}{j\omega\varepsilon}\nabla\left(\nabla \cdot \psi^e\right)\vec{e}_z = \frac{1}{j\omega\varepsilon}\left[\frac{\partial\psi^e}{\partial z\partial x}\hat{x} + \frac{\partial^2\psi^e}{\partial z^2}\hat{z}\right] \tag{3}$$

substituting Eq. (3) in Eq. (1) leads to:

$$E_x = \frac{-\partial\psi^h}{\partial y} + \frac{1}{j\omega\varepsilon}\frac{\partial\psi^e}{\partial x\partial z} \tag{4}$$

$$jE_z = \frac{1}{\omega\varepsilon_0\varepsilon_r}\left[k_0^2\varepsilon_r\psi^e + \frac{\partial^2\psi^e}{\partial z}\right] \tag{5}$$

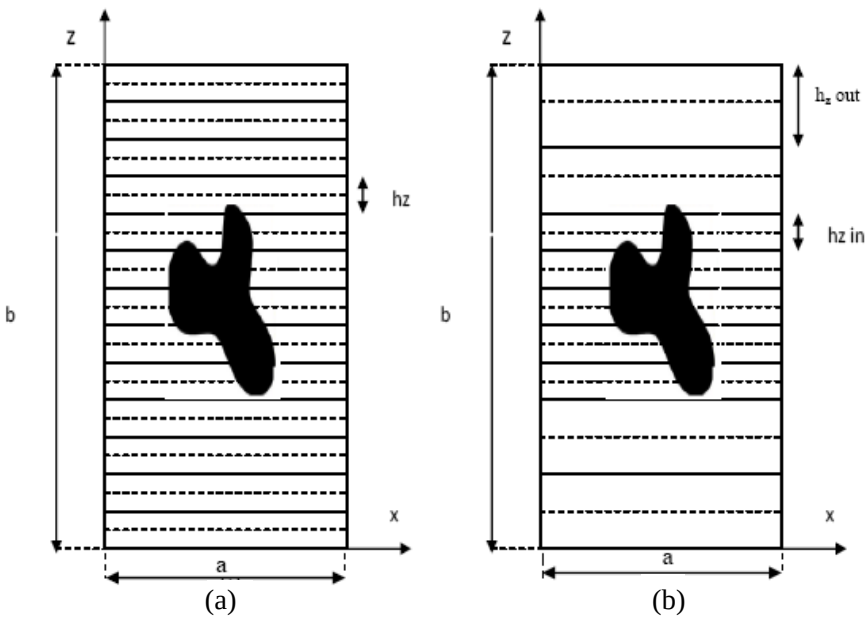

Figure 1. Arbitrarily shaped resonator discretized in z-direction. (a) Equidistant discretization. (b) Non-equidistant discretization.

Applying the same concept for the magnetic field, one gets:

$$\frac{1}{j\omega\mu}\nabla\left(\nabla\cdot\psi^h\right)\vec{e}_z = \nabla\left(\frac{\partial\psi^h}{\partial z}\right) = \frac{1}{j\omega\mu}\left[\frac{\partial\psi^h}{\partial x\partial z}\hat{x} + \frac{\partial^2\psi^h}{\partial z^2}\hat{z}\right] \quad (6)$$

$$H_x = \frac{\partial\psi^e}{\partial y} + \frac{1}{j\omega\mu}\frac{\partial\psi^h}{\partial x\partial z} \quad (7)$$

$$jH_z = \frac{1}{\omega\mu_0}\left[k_0^2\varepsilon_r\psi^h + \frac{\partial^2\psi^h}{\partial z^2}\right] \quad (8)$$

2.2. Discretization

Consider the structure of the arbitrarily shaped microstrip resonators of Fig. 1(a). The first step of the analysis is to slice the resonator structure in the x-y plane along each discretized z line for the two scalar potentials ψ^e and ψ^h separately. This corresponds to a one-dimensional discretization along the z direction.

For arbitrarily shaped resonators with fine details, it is useful to modify the traditional (SSDA) by applying non-equidistant discretization technique as seen in Fig. 1(b). In this figure, most of the discretization lines are concentrated around the irregularities of the metallization sections to reduce the computation time as described in [18, 19]. In this case, the different operators can be expressed as follows:

$$\bar{D}_z^e = r_h D_z r_e, \qquad \bar{D}_z^h = -r_e D_z^t r_h \quad (9)$$

$$P_z^e = -D_z^t D_z, \qquad P_z = -D_z D_z^t \quad (10)$$

where r_e and r_h are defined in [18] and [19].

Equations (9)–(10) represent a system of coupled equations matrices, to convert this system to an uncoupled one; a transformation by a metric T is applied in the form:

$$T^{et}P_z^eT = \lambda_z^e, \qquad T^{ht}P_z^hT^h = \lambda_z^h, \qquad \lambda_z = \delta^2 \quad (11)$$

where T^e and T^h are the matrices of the eigenvectors, and λ_z is the matrix of eigen value.

2.3. Spectral Domain Transformation

For each of these slices, a set of continuous basis functions is then introduced which satisfy the boundary conditions along the x-direction. This step replaces the discretization in the x direction known in the two dimensional MOL. Subsequently, a Fourier transformation is performed to replace the x coordinate in the Helmholtz equation with the spectral term α. The two remaining spatial variables y and z, are

then reduced to only the y variable by applying the transformation procedure known from the one dimensional MOL in the z direction.

The variation of the fields in x-direction is expressed by the spectral factor [20] α_n where:

$$\alpha_n = \frac{n\pi}{a} \tag{12}$$

$$\psi^e(x,y,z) = \psi^e(y,z)\sin\alpha_n x \tag{13}$$

$$\psi^h(x,y,z) = \psi^h(y,z)\cos\alpha_n x \tag{14}$$

Now, the variation of the electric and magnetic potentials in x direction is expressed as the sum of 'sin' and 'cos' functions respectively. Substituting Eqs. (13)–(14) in Eqs. (4), (5), (7) and (8) leads to:

$$E_x = \left(\frac{\alpha_n}{j\omega\varepsilon_0\varepsilon_r}\frac{\partial\psi^e(y,z)}{\partial z} - \frac{\partial\psi^h}{\partial y}\right)\cos\alpha_n x \tag{15}$$

$$jE_Z = \frac{1}{\omega\varepsilon_0\varepsilon_r}\left(\frac{\partial^2\psi^e(y,z)}{\partial z^2} + \varepsilon_r k_0^2\psi^e(y,z)\right)\sin\alpha_n x \tag{16}$$

$$jH_Z = \frac{1}{\omega\mu_0}\left(\frac{\partial^2\psi^h(y,z)}{\partial z^2} + \varepsilon_r k_0^2\psi^h(y,z)\right)\cos\alpha_n x \tag{17}$$

$$H_x = \left(\frac{-\alpha_n}{j\omega\mu_0}\frac{\partial\psi^h(y,z)}{\partial z} + \frac{\partial\psi^e(y,z)}{\partial y}\right)\sin\alpha_n x \tag{18}$$

Taking the Fourier transform of Eqs. (15)–(18), one gets the electric field in the form:

$$\tilde{e}_x(n,y,z) = \frac{\alpha_n}{j\omega\varepsilon_0\varepsilon_r}\frac{\partial\psi^e(y,z)}{\partial z} - \frac{\partial\psi^h(y,z)}{\partial y} \tag{19}$$

$$j\tilde{e}_z(n,y,z) = \frac{1}{\omega\varepsilon_0\varepsilon_r}\left(\frac{\partial^2\psi^{e^2}}{\partial z^2} + \varepsilon_r k_0^2\psi^e\right) \tag{20}$$

and the magnetic field in the form:

$$j\bar{h}_z(n,y,z) = \frac{1}{\omega\mu_0}\left(\frac{\partial^2\psi^h}{\partial z^2} + \varepsilon_r k_0^2\psi^h\right) \tag{21}$$

$$\bar{h}_x(n,y,z) = \frac{-\alpha_n}{j\omega\mu_0}\frac{\partial\psi^h}{\partial z} + \frac{\partial\psi^e}{\partial y} \tag{22}$$

2.4. Discretizing the Wave Equation

Using the Helmholtz equation

$$\frac{\partial^2\psi^{e,h}}{\partial x^2} + \frac{\partial^2\psi^{e,h}}{\partial y^2} + \frac{\partial^2\psi^{e,h}}{\partial z^2} = -k^2\psi^{e,h} \tag{23}$$

and substituting the variation in x direction by the spectral term α in Eqs. (13)–(14), one obtains:

$$\frac{\partial^2\psi^{e,h}}{\partial y^2}+\frac{\partial^2\psi^{e,h}}{\partial z^2}-\left(\alpha_n^2-\varepsilon_r k_0^2\right)\psi^{e,h}=0 \tag{24}$$

Applying the non-equidistant discretization technique in the z-direction to get:

$$\frac{\partial^2\psi^{e,h}}{\partial y^2}-\frac{P_Z}{h_z^2}\psi^{e,h}-\left(\alpha_n^2-\varepsilon_r k_0^2\right)\psi^{e,h}=0 \tag{25}$$

2.5. Wave Equation Transformation

Equation (25) represents a system of ordinary coupled differential equations. A transformation to the principle axis is applied to convert this system of equations to un-coupled ones [3–6], hence,

$$\psi=T\bar{\phi}\qquad \text{where:}\quad T_h^t P_z T_e=\delta^2 \tag{26}$$

$$\frac{\partial^2\bar{\varphi}^{e,h}}{\partial y^2}-\left(\frac{\delta^2}{h_z^2}+\alpha_n^2-\varepsilon_r k_0^2\right)\bar{\varphi}^{e,h}=0 \tag{27}$$

$$\text{or:}\qquad \frac{\partial^2\bar{\varphi}^{e,h}}{\partial y^2}-k_i^2\bar{\varphi}^{e,h}=0\qquad \text{where}\ \ k_i^2=\left(\frac{\delta^2}{h_z^2}+\alpha_n^2-\varepsilon_r k_0^2\right)$$

Eq. (27) has a general solution in the form:

$$\bar{\phi}=A_i\cosh k_{yi}y+B_i\sinh k_{yi}y \tag{28}$$

For any two layers I, II (as seen in Figs. 2(a)):

$$\begin{pmatrix}\vec{\phi}^{e,h}\\ \frac{\partial\varphi^{e,h}}{\partial y}\end{pmatrix}_{y_2}=\begin{pmatrix}\cosh k_{yi}(y_2-y_1) & \sinh k_{yi}(y_2-y_1)\\ k_{yi}\sinh k_{yi}(y_2-y_1) & \cosh k_{yi}(y_2-y_1)\end{pmatrix}\begin{pmatrix}\vec{\phi}^{e,h}\\ \frac{\partial\varphi^{e,h}}{\partial y}\end{pmatrix}_{y_1} \tag{29}$$

which can be written in the form:

$$\begin{bmatrix}\bar{\phi}_{i+1}^{e}\\ \frac{\partial\bar{\phi}_{i+1}^{h}}{\partial y}\\ \frac{\partial\bar{\phi}_{i+1}^{e}}{\partial y}\\ \bar{\phi}_{i+1}^{h}\end{bmatrix}$$

$$=\begin{bmatrix}\cosh ky_i^e t & 0 & \frac{\sinh ky_i^e t}{ky_i^e} & 0\\ 0 & \cosh ky_i^e t & 0 & ky_i\sinh ky_i^e t\\ ky_i\sinh ky_i^e t & 0 & \cosh ky_i^h t & 0\\ 0 & \frac{\sinh ky_i^e t}{ky_i^e} & 0 & \cosh ky_i^h t\end{bmatrix}\begin{bmatrix}\bar{\phi}_i^{e}\\ \frac{\partial\bar{\phi}_i^{h}}{\partial y}\\ \frac{\partial\bar{\phi}_i^{e}}{\partial y}\\ \bar{\phi}_i^{h}\end{bmatrix} \tag{30}$$

2.6. Discretizing and Transforming the Field Equations

Applying the z-direction discretization to Eq. (18):

$$\tilde{e}_x(n,y,z) = \frac{\alpha_n}{j\omega\varepsilon_0\varepsilon_r h_z}\bar{D}_Z\psi^e - \frac{\partial\psi^h}{\partial y} \tag{31}$$

and then transforming Eq. (31) using Eq. (26) one gets:

$$\tilde{\bar{E}}_x(n,y,z) = \frac{\alpha_n\delta}{j\omega\varepsilon_0\varepsilon_r h_z}\bar{\phi}^e - \frac{\partial\bar{\phi}^h}{\partial y} \tag{32}$$

Applying the same procedures to the other field components leads to:

$$\begin{bmatrix} \tilde{\bar{E}}_x \\ j\tilde{\bar{E}}_z \\ j\tilde{\bar{H}}_z \\ \tilde{\bar{H}}_x \end{bmatrix} = \begin{bmatrix} \frac{\alpha_n\delta}{j\omega\varepsilon_0\varepsilon_r h_z} & -I & 0 & 0 \\ \frac{k_0^2\varepsilon_r h_z^2-\delta^2}{\omega\varepsilon_0\varepsilon_r\mu_0 h_z^2} & 0 & 0 & 0 \\ 0 & 0 & 0 & \frac{k_0^2\varepsilon_r h_z^2-\delta^2}{\omega\mu_{0r}h_z^2} \\ 0 & 0 & I & \frac{\delta^t\alpha_n}{j\omega\mu_0 h_z} \end{bmatrix} \begin{bmatrix} \bar{\varphi}^e \\ \frac{\partial\bar{\varphi}^h}{\partial y} \\ \frac{\partial\bar{\varphi}_e}{\partial y} \\ \bar{\varphi}^h \end{bmatrix} \tag{33}$$

2.7. Field Matching

Transforming the field from the any lower interface 'i' to the upper interface '$i+1$' seen in Fig. 2(b) leads to:

$$\begin{bmatrix} \tilde{\bar{E}}_x \\ j\tilde{\bar{E}}_z \\ j\tilde{\bar{H}}_z \\ \tilde{\bar{H}}_x \end{bmatrix}_{I+1} = \Pi_{i=1}^{L_1} R_i Q_i R_i^{-1} \begin{bmatrix} \tilde{\bar{E}}_x \\ j\tilde{\bar{E}}_z \\ j\tilde{\bar{H}}_z \\ \tilde{\bar{H}}_x \end{bmatrix}_I \tag{34}$$

where Eq. (34) represents the recurrence equations for any two subsequent layers.

Transforming from the lower interface 'L' to the lower resonator interface '---' as observed from Fig. 2(a):

$$\begin{bmatrix} \tilde{\bar{E}}_- \\ \tilde{\bar{H}}_- \end{bmatrix} = \begin{bmatrix} y_1^I & y_2^I \\ y_3^I & y_4^I \end{bmatrix} \begin{bmatrix} \tilde{\bar{E}}_L \\ \tilde{\bar{H}}_L \end{bmatrix} \tag{35}$$

$$\text{where : } y_1 = y_4 = \begin{bmatrix} \cosh k_{yi}t & 0 \\ 0 & \cosh k_{yi}t \end{bmatrix} \tag{36}$$

$$y_2 = \begin{bmatrix} \frac{h_z\delta^2\alpha^2\sin\gamma t-\gamma^2\omega^2\varepsilon_0\varepsilon_r h_z^3\mu_0\sinh\gamma t}{\gamma\omega\varepsilon_0\varepsilon_r h_z(\varepsilon_r k_0^2 h_z^2-\delta^2)} & \frac{\delta\alpha}{j\omega\varepsilon_0\varepsilon_r h_z}\frac{\sinh\gamma t}{\gamma} \\ \frac{j\delta\alpha}{\omega\varepsilon_0\varepsilon_r h_z}\frac{\sinh\gamma t}{\gamma} & \frac{\varepsilon_r k_0^2 h_z^2-\delta^2}{\omega\varepsilon_0\varepsilon_r h_z^2}\frac{\sinh\gamma t}{\gamma} \end{bmatrix} \tag{37}$$

$$y_3 = \begin{bmatrix} \frac{\varepsilon_r k_0^2 h_z^2-\delta^2}{\omega\mu_{0r}h_z^2}\frac{\sinh k_y t}{k_y} & \frac{\varepsilon_r k_0^2 h_z^2-\delta^2}{\omega\varepsilon_0\varepsilon_r h_z^2}\frac{\sinh k_y t}{k_y} \\ \frac{j\delta\alpha}{\omega\mu_{0r}h_z}\frac{\sinh k_y t}{k_y} & \frac{k_y^2\omega h^2 z^2\mu_0\varepsilon_0\varepsilon_r-\delta^2\alpha^2}{\omega\mu_0(\varepsilon_r k_0^2 h_z^2-\delta^2)k_y}\frac{\sinh k_y t}{k_y} \end{bmatrix} \tag{38}$$

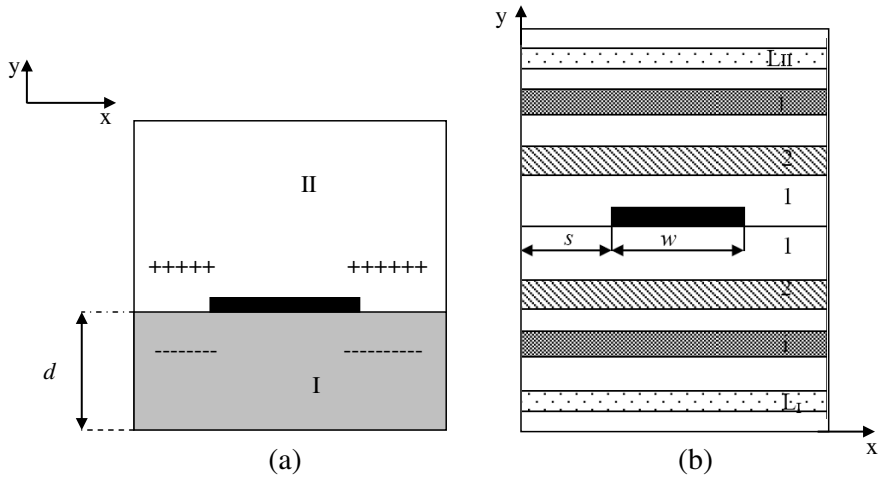

Figure 2. Field transformation on multiple dielectric layers.

Transforming from the upper interface 'U' to the upper resonator interface '+++' as observed from Fig. 2(a):

$$\begin{bmatrix} \tilde{\tilde{E}}_+ \\ \tilde{\tilde{H}}_+ \end{bmatrix} = \begin{bmatrix} y_1^{II} & -y_2^{II} \\ -y_3^{II} & y_4^{II} \end{bmatrix} \begin{bmatrix} \tilde{\tilde{E}}_U \\ \tilde{\tilde{H}}_U \end{bmatrix} \tag{39}$$

Applying the boundary conditions at the lower interface 'L' and upper interface 'U' leads to:

$$\begin{bmatrix} \tilde{\tilde{Z}}_1 & \tilde{\tilde{Z}}_2 \\ \tilde{\tilde{Z}}_3 & \tilde{\tilde{Z}}_4 \end{bmatrix} \begin{bmatrix} -\tilde{\tilde{J}}_x \\ \tilde{\tilde{J}}_z \end{bmatrix} = \begin{bmatrix} \tilde{\tilde{E}}_x \\ j\tilde{\tilde{E}}_z \end{bmatrix} \tag{40}$$

2.8. Backward Transformation

Transforming Eq. (40) back to the original domain leads to:

$$\begin{bmatrix} T^{ht} & \\ & T^{et} \end{bmatrix} \begin{bmatrix} \tilde{\tilde{Z}}_1 & \tilde{\tilde{Z}}_2 \\ \tilde{\tilde{Z}}_3 & \tilde{\tilde{Z}}_4 \end{bmatrix} \begin{bmatrix} T^h & \\ & T^e \end{bmatrix} \begin{bmatrix} -\tilde{J}_x \\ \tilde{J}_z \end{bmatrix} = \begin{bmatrix} \tilde{E}_x \\ j\tilde{E}_z \end{bmatrix} \tag{41}$$

2.9. Boundary Conditions

Applying the boundary conditions at the lines through the metallization to get:

$$\begin{bmatrix} \tilde{Z}_1(f,\alpha) & \tilde{Z}_2(f,\alpha) \\ \tilde{Z}_3(f,\alpha) & \tilde{Z}_4(f,\alpha) \end{bmatrix}^r \begin{bmatrix} -\tilde{J}_x \\ \tilde{J}_z \end{bmatrix} = \begin{bmatrix} 0 \\ 0 \end{bmatrix} \tag{42}$$

and through the dielectric lines

$$\begin{bmatrix} \tilde{Z}_1(f,\alpha) & \tilde{Z}_2(f,\alpha) \\ \tilde{Z}_3(f,\alpha) & \tilde{Z}_4(f,\alpha) \end{bmatrix}^o \begin{bmatrix} -\tilde{J}_x \\ \tilde{J}_z \end{bmatrix} = \begin{bmatrix} \tilde{E}_x \\ j\tilde{E}_z \end{bmatrix} \tag{43}$$

2.10. Moment Method

Assume that the current 'J' is defined with a known function with unknown coefficients in the form [3]

$$\tilde{J}_z^{k^e} = b_i^{k^e} \sum_{i=1}^{n_{jz}} \tilde{J}_{zi}(\alpha) \tag{44}$$

$$\tilde{J}_x^{k^h} = a_j^{k^h} \sum_{j=1}^{n_{J_x}} \tilde{J}_{xj}(\alpha) \tag{45}$$

where 'i' is the number of the basis functions and 'k' the line number. The functions J_{zF} and J_{xF} are chosen to satisfy the boundary conditions at the strip and at the edges of the strip lines.

$$J_{z_i}^{k^e}(x) = \left\{ \begin{array}{ll} \dfrac{b_i^{k^e} \cos\left[\frac{i\pi(x-s)}{W}\right]}{\sqrt{1-\left[\frac{2}{W}(x-s)-1\right]^2}} & i = 0, 2, 4, 6, \ldots \\ \dfrac{b_i^{k^e} \sin\left[\frac{i\pi(x-s)}{W}\right]}{\sqrt{1-\left[\frac{2}{W}(x-s)-1\right]^2}} & i = 1,\ 3,\ 5, \ldots \end{array} \right\} \tag{46}$$

$$J_{x_j}^{k^h}(x) = \left\{ \begin{array}{ll} \dfrac{a_j^{k^h} \cos\left[\frac{j\pi(x-s)}{W}\right]}{\sqrt{1-\left[\frac{2}{W}(x-s)-1\right]^2}} & j = 1,\ 3,\ 5, \ldots \\ \dfrac{a_j^{k^h} \sin\left[\frac{j\pi(x-s)}{W}\right]}{\sqrt{1-\left[\frac{2}{W}(x-s)-1\right]^2}} & j = 0, 2, 4, 6, \ldots \end{array} \right\} \tag{47}$$

To solve Eqs. (42)–(43) the current functions must be transformed by the Fourier transform to obtain [3]:

$$\tilde{J}_{z_i}(\boldsymbol{\alpha}) = \left\{ \begin{array}{l} \dfrac{\pi}{4} W e^{j(s+(W/2))\alpha} (-1)^{\frac{1}{2}} \\ \left[J_0\left(\dfrac{\alpha W}{2} + \dfrac{i\pi}{2}\right) + J_0\left(\dfrac{\alpha W}{2} - \dfrac{i\pi}{2}\right) \right] \\ \qquad\qquad i = 0, 2, 4, 6, \ldots \\ \dfrac{\pi}{4} W e^{j(s+(W/2))\alpha} (-1)^{\frac{(i-1)}{2}} \\ \left[J_0\left(\dfrac{\alpha W}{2} + \dfrac{i\pi}{2}\right) + J_0\left(\dfrac{\alpha W}{2} - \dfrac{i\pi}{2}\right) \right] \\ \qquad\qquad i = 1, 3, 5, \ldots \end{array} \right\} \tag{48}$$

$$\tilde{J}_{x_j}(\boldsymbol{\alpha}) = \left\{ \begin{array}{l} \dfrac{\pi}{4} w e^{j(s+(W/2))\alpha} (-1)^{\frac{j}{2}} \\ \left[J_0\left(\dfrac{\alpha W}{2} + \dfrac{j\pi}{2}\right) - J_0\left(\dfrac{\alpha W}{2} - \dfrac{j\pi}{2}\right) \right] \\ \qquad\qquad j = 0, 2, 4, 6, \ldots \\ \dfrac{\pi}{4} w e^{j(s+(W/2))\alpha} (-1)^{\frac{(j+1)}{2}} \\ \left[J_0\left(\dfrac{\alpha W}{2} + \dfrac{j\pi}{2}\right) - J_0\left(\dfrac{\alpha W}{2} - \dfrac{j\pi}{2}\right) \right] \\ \qquad\qquad j = 1, 3, 5, \ldots \end{array} \right\} \tag{49}$$

where 'J_0' is the zero order Bessel function. Eq. (42) becomes:

$$\begin{bmatrix} \tilde{Z}_1(f,\alpha)\tilde{J}_{xj}(\alpha) & \tilde{Z}_2(f,\alpha)\tilde{J}_{zi}(\alpha) \\ \tilde{Z}_3(f,\alpha)\tilde{J}_{xj}(\alpha) & \tilde{Z}_4(f,\alpha)\tilde{J}_{zi}(\alpha) \end{bmatrix}^r \begin{bmatrix} a_j^{k^h} \\ b_i^{k^e} \end{bmatrix} = \begin{bmatrix} 0 \\ 0 \end{bmatrix} \tag{50}$$

Now, Galerkin technique is applied to solve Eq. (50). Using basis functions $\tilde{J}_{x_j}(\alpha)$ for the first part of Eq. (49) and $\tilde{J}_{z_i}(\alpha)$ for the second part of the equation to get:

$$\begin{bmatrix} \sum\limits_{n=1}^{N} \tilde{J}_{x_j}(\alpha)\tilde{Z}_1(f,\alpha)\tilde{J}_{x_j}(\alpha) & \sum\limits_{n=1}^{N} \tilde{J}_{z_i}(\alpha)\tilde{Z}_2(f,\alpha)\tilde{J}_{z_i}(\alpha) \\ \sum\limits_{n=1}^{N} \tilde{J}_{x_j}(\alpha)\tilde{Z}_3(f,\alpha)\tilde{J}_{x_j}(\alpha) & \sum\limits_{n=1}^{N} \tilde{J}_{z_i}(\alpha)\tilde{Z}_4(f,\alpha)\tilde{J}_{z_i}(\alpha) \end{bmatrix}^r \begin{bmatrix} a_j^{k^h} \\ b_i^{k^e} \end{bmatrix} = \begin{bmatrix} 0 \\ 0 \end{bmatrix} \tag{51}$$

which can be written in the form:

$$\begin{bmatrix} z_1(f) & z_2(f) \\ z_3(f) & z_4(f) \end{bmatrix}^r \begin{bmatrix} a_j^{k^h} \\ b_i^{k^e} \end{bmatrix} = \begin{bmatrix} 0 \\ 0 \end{bmatrix} \tag{52}$$

Equation (52) is a determinant equation which is satisfied at the resonance frequency of the structure. The second step is obtaining the unknown current coefficient a_j and b_i from which the current can be calculated using Eqs. (46)–(47) from which the other field components can be calculated.

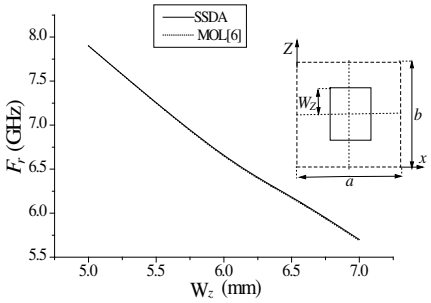

Figure 3. Effect of changing W_z on the resonance frequency of the rectangular resonator $\varepsilon_r = 3.82$, $d = 0.66\,\text{mm}$, $a = 10\,\text{mm}$, $s = 2\,\text{mm}$, $W_x = 3\,\text{mm}$, $J_x = 3$, $J_z = 1$.

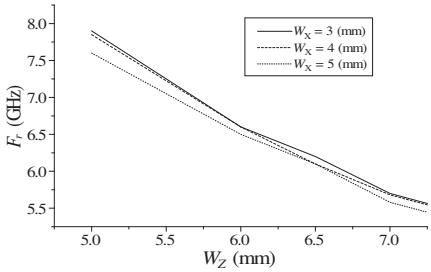

Figure 4. Effect of changing W_z and W_x on the resonance frequency of the rectangular resonator $\varepsilon_r = 3.82$, $d = 0.66\,\text{mm}$, $a = 10\,\text{mm}$, $s = 2\,\text{mm}$, $W_x = 3\,\text{mm}$, $J_x = 3$, $J_z = 1$.

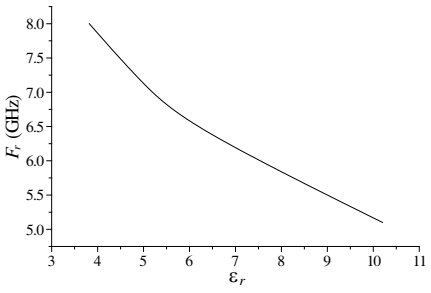

Figure 5. Effect of changing ε_r on the resonance frequency of the rectangular resonator $W_z = 5\,\text{mm}$, $W_x = 3\,\text{mm}$, $d = 0.66\,\text{mm}$, $a = 10\,\text{mm}$, $s = 2\,\text{mm}$, $J_x = 3$, $Jz = 1$.

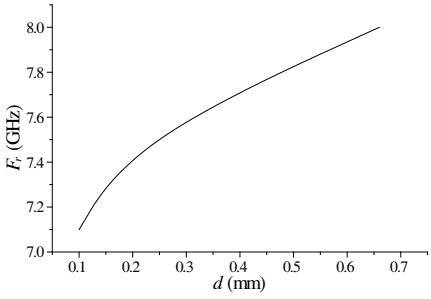

Figure 6. Effect of changing the substrate depth "d" on the resonance frequency of the rectangular resonator $\varepsilon_r = 3.82$, $a = 10\,\text{mm}$, $s = 2\,\text{mm}$, $W_z = 5\,\text{mm}$, $W_x = 3\,\text{mm}$, $J_x = 3$, $J_z = 1$.

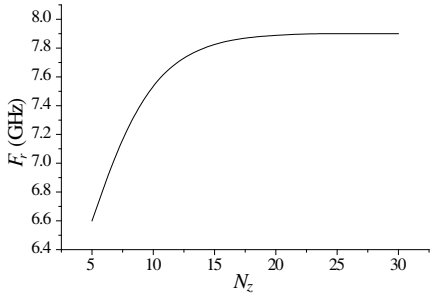

Figure 7. Effect of changing the number of discretization lines N_z on the resonance frequency of the rectangular resonator $\varepsilon_r = 3.82$, $d = 0.66\,\text{mm}$, $a = 10\,\text{mm}$, $s = 2\,\text{mm}$, $W_z = 5\,\text{mm}$, $W_x = 3\,\text{mm}$, $J_x = 3$, $J_z = 1$.

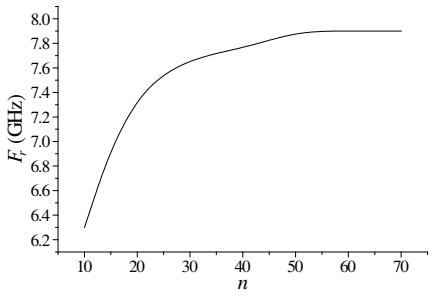

Figure 8. Effect of the changing the number of spectral terms n on the resonance frequency of the rectangular resonator $\varepsilon_r = 3.82$, $d = 0.66\,\text{mm}$, $a = 10\,\text{mm}$, $s = 2\,\text{mm}$, $W_z = 5\,\text{mm}$, $W_x = 3\,\text{mm}$, $J_x = 3$, $J_z = 1$.

3. NUMERICAL RESULTS

To check the validity of the method and the accuracy of the program, the program is applied first on a rectangular microstrip resonator for resonance frequency calculations. The results were compared with those in [6] and [14] where good agreement is found as seen in Fig. 3. It is also observed in this figure that the resonance frequency F_r increases as W_Z decreases. Fig. 4 shows that, the resonator width W_X is slightly affecting the resonance frequency of this resonator. Figs. 5–6 show the effect of the substrate parameters on the resonance frequency of the resonator, and it is seen from those figures that the resonance frequency decreases with the increase of dielectric permittivity ε_r and the decrease of dielectric depth "d". This is expected because the increase of the dielectric permittivity ε_r or the decrease of the dielectric depth d makes the field more confined in the substrate material.

From Figs. 7–9, it is seen that the main factors affecting the accuracy of the results are

1. Number of discretization lines Nz
2. Number of the spectral terms $\alpha(n)$
3. Number of the basis functions of the current J_X, J_Z

- **Number of discretization lines**

As seen in Fig. 7, the results converges to the right solution as the number of the discretization lines increases. For the rectangular

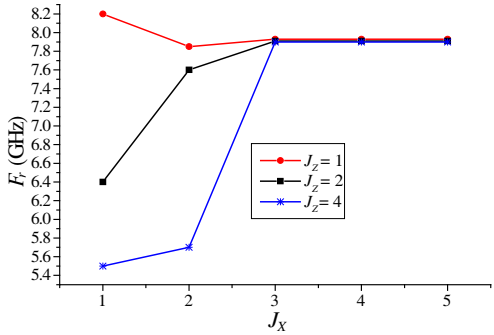

Figure 9. Effect of changing the number of the basis functions J_z and J_x on the resonance frequency of the rectangular resonator $\varepsilon_r = 3.82$, $d = 0.66\,\text{mm}$, $a = 10\,\text{mm}$, $s = 2\,\text{mm}$, $W_z = 5\,\text{mm}$, $W_x = 3\,\text{mm}$.

resonator under study, it is found that 20×20 lines are needed to reach the converged results using the conventional 2-D (MOL), and using the conventional (SSDA), it is found that 20 lines are sufficient to reach the converged results. While, when using non-equidistant discretization for the modified (SSDA) the number of lines needed to pass through the metallization part of the resonator are only 10 lines for reaching the converged results and from the previous results, it is found that using the modified (SSDA) algorithm, the number of discretization lines decreases from 400 lines in the conventional (MOL) to 14 lines only in this algorithm. This leads accordingly to a large decrease in the computation time reaching less than 10%. As an example, the conventional MOL, SSDA and the modified SSDA are applied to the rectangular shape resonator. It is found that the CPU times of execution of the methods to reach the converged results are: 300 : 50 : 10 ms respectively (using the same processor), which is directly proportional to the number of discretization lines, and the corresponding size of arrays.

- **Number of the Spectral Terms** $\alpha(n)$

It is shown in Fig. 8 that the convergence of the resonant frequency is reached as the number of the spectral terms $\alpha(n)$ increases. It is also found that $n = 60$ is a sufficient number of the spectral terms to reach the exact solution.

- **Number of the basis functions of the current** J_X**,** J_Z

It is seen in Fig. 9 that the appropriate number of the basis functions in the x-component to reach the converged results are $J_X = 3$. While, the

change in the number of the basis functions in z-component J_Z slightly affect the numerical solution. Hence, the suitable number of the basis functions can be assumed as $J_X = 3$ and $J_Z = 1$ for rectangular shape resonator however highly complicated shapes may require larger values of J_X to obtain accurate results.

After checking the main factors affecting the accuracy of the numerical results of the rectangular resonator, the algorithm is applied

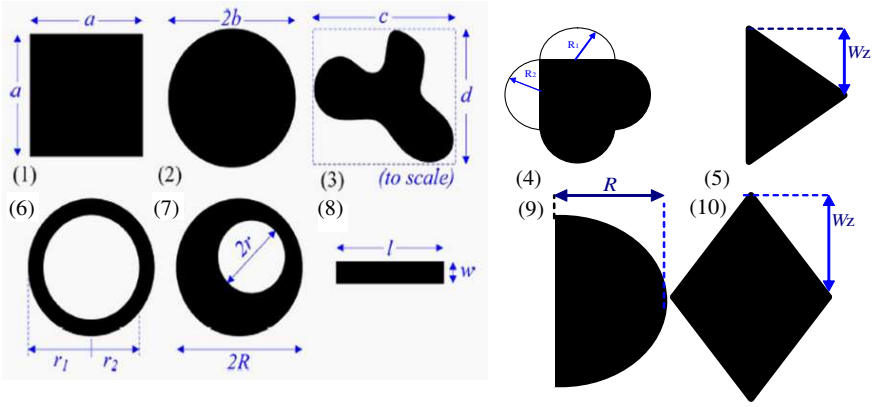

Figure 10. Ten different arbitrary shaped resonators (1) rectangular resonator, (2) circular resonator, (3) arbitrary resonator, (4) arbitrary circular resonator, (5) half rhombic resonator, (6) ring resonator, (7) arbitrary ring resonator, (8) strip line resonator, (9) half circular resonator, (10) rhombic resonator.

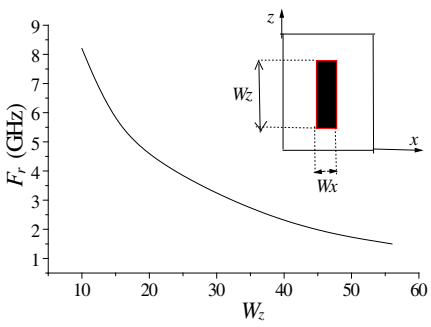

Figure 11. Effect of changing W_z on the resonance frequency of the strip line resonator $\varepsilon_r = 3.82$, $d = 0.66\,\text{mm}$, $a = 10\,\text{mm}$, $s = 2\,\text{mm}$, $W_x = 3\,\text{mm}$, $J_x = 3$, $J_z = 1$.

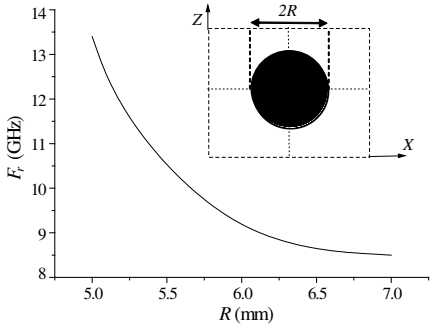

Figure 12. Effect of changing R on the resonance frequency of the ring resonator $\varepsilon_r = 3.82$, $d = 0.66\,\text{mm}$, $a = 10\,\text{mm}$, $s = 2\,\text{mm}$, $Jx = 3$, $Jz = 1$.

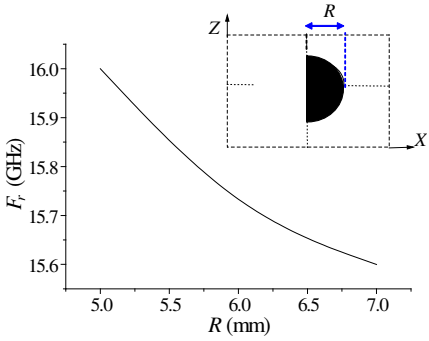

Figure 13. Effect of changing R on the resonance frequency of the half-ring resonator $\varepsilon_r = 3.82$, $d = 0.66\,\text{mm}$, $a = 10\,\text{mm}$, $s = 2\,\text{mm}$, $J_x = 3$, $J_z = 1$.

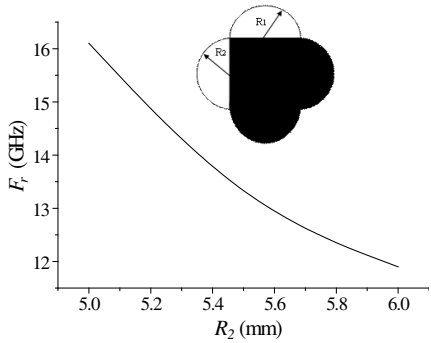

Figure 14. Effect of changing R_2 on the resonance frequency of the arbitrarily circular shaped resonator $R_1 = 2.0\,\text{mm}$, $\varepsilon_r = 3.82$, $d = 0.66\,\text{mm}$, $a = 10\,\text{mm}$, $s = 2\,\text{mm}$, $J_x = 3$, $J_z = 1$.

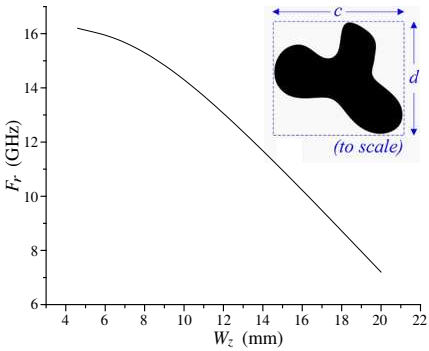

Figure 15. Effect of changing W_z on the resonance frequency of the arbitrarily shaped resonator $\varepsilon_r = 3.82$, $d = 0.66\,\text{mm}$, $a = 10\,\text{mm}$, $s = 2\,\text{mm}$, $J_x = 3$, $J_z = 1$.

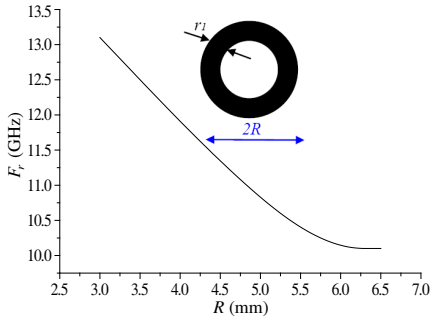

Figure 16. Effect of changing the radius R on the resonance frequency of the ring resonator $\varepsilon_r = 3.82$, $d = 0.66\,\text{mm}$, $a = 10\,\text{mm}$, $s = 2\,\text{mm}$, $J_x = 3$, $J_z = 1$, $r_1 = 0.5\,\text{mm}$.

for the design and resonance frequency calculations of the other shapes of Fig. 10. These structures are: circular resonator (2), arbitrary resonator (3), arbitrary circular resonator (4) half rhombic resonator (5), ring resonator (6), Arbitrary ring resonator (7) strip line resonator (8) , half circular resonator (9) and rhombic resonator (10).

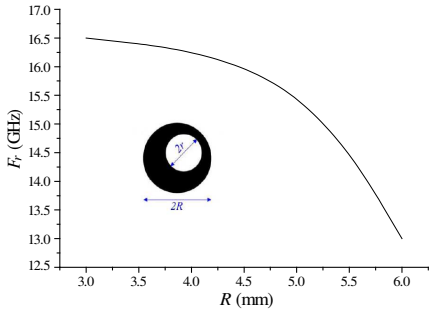

Figure 17. Effect of changing the radius R on the resonance frequency of the arbitrary ring resonator $\varepsilon_r = 3.82$, $a = 10\,\text{mm}$, $d = 0.66\,\text{mm}$, $s = 2\,\text{mm}$, $J_x = 3$, $J_z = 1$, $r = 0.5\,\text{mm}$.

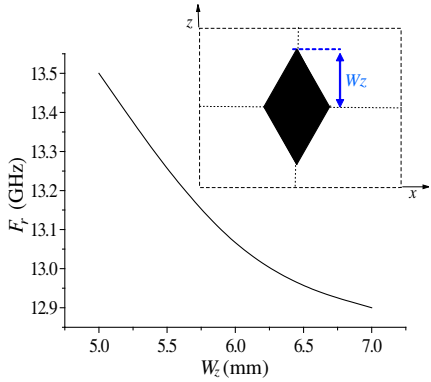

Figure 18. Effect of changing W_z on the resonance frequency of the rhombic resonator $\varepsilon_r = 3.82$, $d = 0.66\,\text{mm}$, $a = 10\,\text{mm}$, $s = 2.5\,\text{mm}$, $W_x = 3\,\text{mm}$, $J_x = 3$, $J_z = 1 = 1\,\text{mm}$.

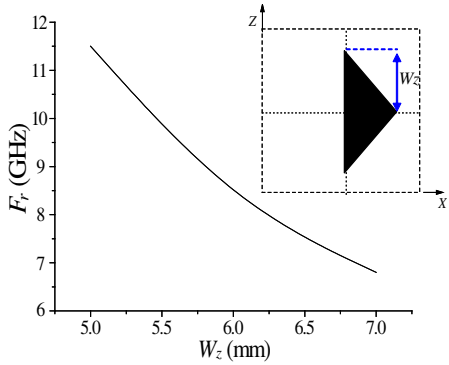

Figure 19. Effect of changing W_z on the resonance frequency of the half-rhombic resonator $\varepsilon_r = 3.82$, $d = 0.66\,\text{mm}$, $a = 10\,\text{mm}$, $s = 2.5\,\text{mm}$, $s = 2.5\,\text{mm}$, $W_x = 2.5\,\text{mm}$, $J_x = 3$, $J_z = 1$.

For the design purposes, all resonators seen in Fig. 10 are adjusted to have resonance frequencies equal to each other as possible [17]. All figures of resonators are chosen to have the same dielectric materials and to have nearly the same dimensions along the z direction. The dependence of the resonant frequency upon the most effective dimension of these resonators is shown in Figs. 11–19. It is also noticed from these figures that regardless to the shape of the

resonator, the resonance frequency decreases as the effective dimension of the resonator increases. Considering the resonator structures which have non-uniform metallic distribution in the resonator patch like arbitrary shaped resonator (3), ring resonator (6) and arbitrary ring resonator (7), the current distribution functions are proposed in the

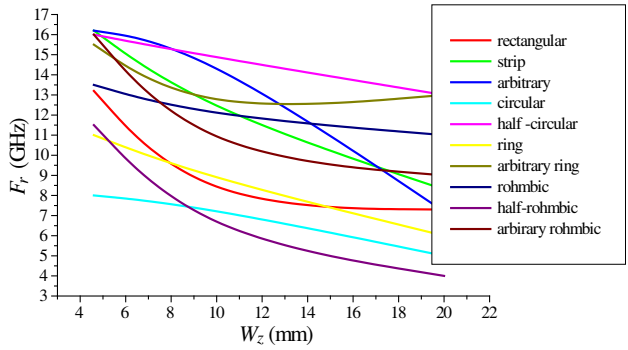

Figure 20. Design curves for different 10 arbitrary shaped resonators using the same substrate material $\varepsilon_r = 3.82$, $d = 0.66\,\text{mm}$, $a = 10\,\text{mm}$ and having nearly the same z dimensions.

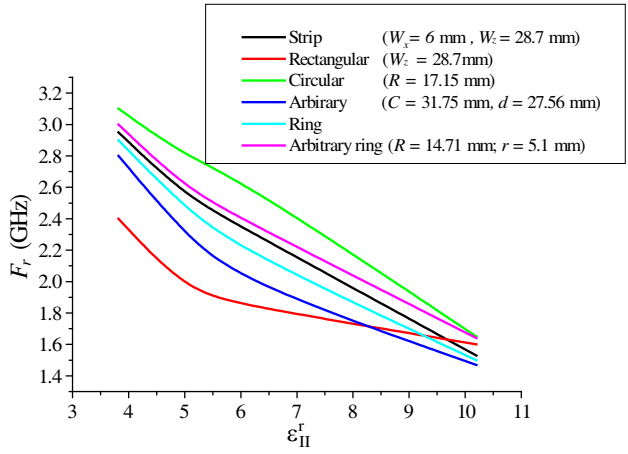

Figure 21. Design curves for the six different arbitrary shaped resonators using different material with the same dielectric depth $d = 1.27\,\text{mm}$.

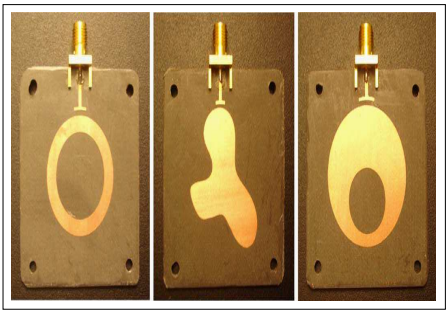

Figure 22. Fabrication of three arbitrary shaped resonators having tiny details and having different dielectric metallization distribution [17].

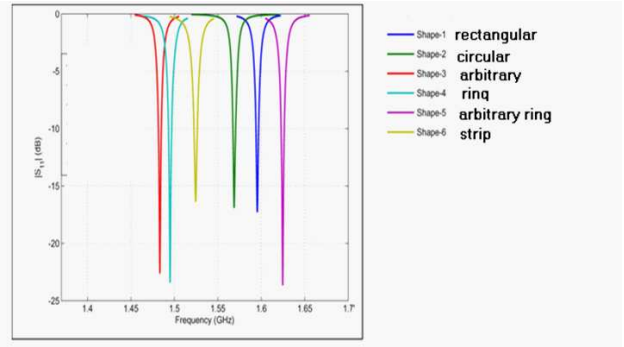

Figure 23. Resonance frequency measurements for the six arbitrary shaped resonators [17].

form:

$$\tilde{J}^{k^e}_{z_i} = \sum_{v=1}^{n_x} \sum_{i=1}^{n_{J_z}} b_i^{k^e} \tilde{J}_{zF}(\alpha) \tag{53}$$

$$\tilde{J}^{k^h}_{x_j} = \sum_{v=1}^{n_x} \sum_{j=1}^{n_{J_x}} a_j^{k^h} \tilde{J}_{xF}(\alpha) \tag{54}$$

where n_x is the number of metallization lines for each discretized line along the z direction.

Figure 20 shows that, for a fixed W_Z, the half ring resonator has the highest resonance frequency of all studied resonator structures. Fig. 21 represents the effect of changing the dielectric

Table 1. Comparison between calculated and measurements results [17] for six resonator shapes: Strip resonator ($W_x = 6\,\text{mm}$, $W_z = 28.7\,\text{mm}$), Rectangular resonator ($W_z = 28.7\,\text{mm}$), Circular resonator ($R = 17.15\,\text{mm}$), Arbirary resonator ($C = 31.75\,\text{mm}$, $d = 27.56\,\text{mm}$), Ring resonator ($R = 12.74\,\text{mm}$, $r1 = 6.74\,\text{mm}$), Arbitrary ring resonator ($R = 14.71\,\text{mm}$, $r = 5.1\,\text{mm}$).

	Strip	Rectangular	Circular	Arbitrary shape	Ring	Arbitrary ring
Calculated f_r	1.53 (GHz)	1.6 (GHz)	1.59 (GHz)	1.47 (GHz)	1.5 (GHz)	1.64 (GHz)
Measured f_r	1.52 (GHz)	1.59 (GHz)	1.57 (GHz)	1.48 (GHz)	1.49 (GHz)	1.62 (GHz)

material on the resonance frequency of six arbitrary shaped resonators given in Fig. 10. Figs. 22, shows the fabrication of arbitrary shaped resonator, ring resonator and arbitrary ring resonator [17] which have tiny details in the resonator patch. Fig. 23 shows the results of resonance frequency measurements for rectangular, circular, arbitrary, ring, arbitrary ring and strip resonators respectively. It is observed from Figs. 21, 23 and Table 1 that good agreement is found between measured [17] and calculated results with F_r ranging from 1.47–1.62 GHz for the six different tested resonator structures which have dielectric material of $\varepsilon_r = 10.2$ and $d = 1.27\,\text{mm}$.

4. CONCLUSION

In this paper, the analysis of the space spectral domain approach (SSDA) is enhanced by non-equidistant (MOL) discretization and the spectral domain analysis of the current distribution is developed. The modifications of the (SSDA) enable the method to be applied for arbitrary shaped structures that cannot be easily solved using the conventional method of lines (MOL) or (SSDA). The resonance frequencies of ten arbitrary shaped resonators with different metallization distribution are obtained using this modified method. Good agreement is found between numerical and experimental results. The dependence of these resonance frequencies upon the most effective dimensions of these resonators is investigated. It is concluded that using the modified (SSDA) with non equidistant decritization reduces the computation time to less than 10% if compared with that of the traditional MOL algorithm.

REFERENCES

1. Hong, J. G. and M. J. Lancaster, *Microstrip Filters for RF/Microwave Applications*, Wiley-Blackwell, New York, 2001.
2. Lee, T., *Planar Microwave Engineering: A Practical Guide to Theory, Measurement, and Circuits*, Cambridge, Cambridge Univ., UK, 2004.
3. Pregla, R. and W. Pascher, "The method of lines," *Numerical Techniques for Microwave and Millimeter Wave Passive Structures*, T. Itoh, Editor, 381–446, John Wiley & Sons, Wiley Pub., New York, 1989.
4. Schulz, U. and R. Pregla, "A new technique for the analysis of the dispersion characteristics of planar waveguides," *Arch Elec. Ubertragung*, Vol. 34, 169–173, 1980.
5. Schulz, U. and R. Pregla, "A new technique for the analysis of the dispersion characteristics of planar waveguides and its application to microstrips with tuning septums," *Radio Sci.*, Vol. 16, 1173–1178, 1981.
6. Worm, S. B. and R. Pregla, "Hybrid mode analysis of arbitrarily shaped planar microwave structures by the method of lines," *IEEE Trans. on Microwave Theory and Techniques*, Vol. 32, 191–196, 1984.
7. Vietzorreck, L. and R. Pregla, "Hybrid analysis of 3-D MMIC elements by the methods of lines," *IEEE Trans. on Microwave Theory and Techniques*, Vol. 44, 2580–2586, 1996.
8. Pregla, R., "Analysis of planar microwave and millimeter wave circuits with anisotropic layers based on Generalized transmission line equation and on the method of lines," *IEEE MTT-S, Int. Symp. Dig.*, 125–128, Boston, USA, Jun. 2000.
9. Pregla, R. and S. F. Helfert, "Modelling of waveguide circuits based on generalized transmission line equations and impedance/admittance transformation concept," *XI Int. Symp. on Theoretical Electrical Engineering*, Linz, Austria, Aug. 2001.
10. Vietzorreck, L. and R. Pregla, "Analysis of Discontinuities in microwave circuits with a new eigenmode algorithm based on the method of lines," *25th Eur. Microwave Conf.*, 804–808, Bologna, Italy, Sept. 1995.
11. Le Floch, J.-M., M. E. Tobar, D. Cros, and J. Krupka, "High Q-factor distributed bragg reflector resonators with reflectors of arbitrary thickness," *IEEE Trans. Ultrason. Ferroelec. Freq. Contr.*, Vol. 54, No. 12, 2689–2695, 2007.
12. Le Floch, J.-M., M. E. Tobar, D. Mouneyrac, D. Cros, and J.

Krupka, "Discovery of Bragg confined hybrid modes with high Q-factor in a hollow dielectric resonator," *Applied Physics Letters*, Vol. 91, No. 14, 142907, 2007.

13. Wu, K. and R. Vahldieck, "A new method of modeling three-dimensional MICNMIC circuits: The space-spectral domain approach," *IEEE Trans. MU*, Vol. 32, No. 9, 1309–1318, Sept. 1990.
14. Wu, K., M. Yu, and R. Vahldieck, "Rigorous analysis of 3-D planar circuits discontinuities using the space-spectral domain approach (SSDA)," *IEEE Trans. on Microwave Theory and Tech.*, Vol. 40, No. 7, 1475–1483, Jul. 1992.
15. Gupta, N. and M. Singh, "The space spectral domain technique applied to a fine line configuration," *IEEE Microwave and Guided Wave Lett.*, Vol. 3, No. 5, 125–126, 1993.
16. Naji, A. and P. Warr, "Independence of the unloaded Q of a planar electromagnetic resonator from its shape," *IEEE Trans. on Microwave Theory and Tech.*, Vol. 60, No. 8, 2370–2377, Aug. 2012.
17. Diestel, H. and S. Worm, "Analysis of hybrid field problems by the method of lines with nonequidistant discretization," *IEEE Trans. on Microwave Theory and Techniques*, Vol. 32, 663–638, 1984.
18. Hashish, E. A. and H. A. Saker, "Full-wave analysis of a wide band parallel cascaded band pass filter using the novel method of lines," *National Radio Science Conference (NRSC)*, NTI, Cairo, Egypt, Mar. 16–18, 2004.
19. Jansen, R. H., "The spectral domain approach for microwave integrated circuits," *IEEE Trans. on Microwave Theory Tech.*, Vol. 33, 1043–1056, 1985.